*Proc. Natl. Acad. Sci. USA*
Vol. 91, pp. 11709–11713, November 1994
Neurobiology

# Disruption of the compacted myelin sheath of axons of the central nervous system in proteolipid protein-deficient mice

(*Plp* gene targeting/knock out of expression/abolished membrane apposition)

DETLEV BOISON AND WILHELM STOFFEL†

Institut für Biochemie, Medizinische Fakultät, Universität zu Köln, Joseph-Stelzmann-Strasse 52, D-50931 Cologne, Germany

*Communicated by Alexander G. Bearn, August 23, 1994*

ABSTRACT **The isoproteins proteolipid protein (PLP) and DM20, the two major integral membrane proteins of central nervous system (CNS) myelin, are encoded by a single gene on the X chromosome and show a different developmental expression pattern. To investigate their functions in myelin structure and myelination, we produced transgenic mice carrying a targeted alteration of the X chromosome-linked *Plp* gene containing a deletion within exon III, mimicking DM20, and a *neo* cassette in reverse orientation within intron III. Here we show that the antisense integration of the *neo* cassette disrupts the expression of the *Plp* gene. The ultrastructure of the multilayer myelin sheath of all axons in the CNS of hemizygous male or homozygous female PLP/DM20-deficient mice is highly disordered. The apposition of the extracytoplasmic surfaces and thereby the intraperiod dense line is lacking. The disrupted assembly of the myelin sheath leads to a profound reduction of conductance velocities of CNS axons, impairments in neuromotor coordination, and behavioral changes.**

The isoproteins proteolipid protein (PLP; 30 kDa) and DM20 (26 kDa) are synthesized by oligodendrocytes as the two major integral proteins of myelin membranes of the central nervous system (CNS) (1). A four-transmembrane-helix topology in the lipid bilayer has been assessed biochemically (2). As structural membrane components of the highly ordered membrane system, they are believed to be responsible, together with myelin basic proteins, for the compaction of the myelin membrane, which provides the insulation of axons and high electric conductance of axons of the CNS. The *Plp* gene has a length of 17.4 kb and is located on chromosome Xq22.3 (3). It contains seven exons coding for 276 amino acids (4, 5). DM20 is an alternative splice product of the *Plp* primary transcript, in which 105 bp at the 3′ end of exon III are deleted due to the activation of a cryptic splice site (6). PLP shows a high degree of evolutionary conservation (7) with a complete amino acid identity between mouse, rat, and man. The highly conserved PLP structure may explain a low mutation tolerance, as evidenced by a large and divergent array of naturally occurring point mutations within the *Plp* gene in different species including man (8). The pleiotropic phenotype in these generally lethal dysmyelinoses results from the apoptosis of oligodendrocytes during the myelination period. The molecular events of these fatal point mutations leading to oligodendrocyte death are not yet understood in detail. Functions other than structural functions have been attributed to PLP/DM20, such as ion and neurotransmitter channel and adhesive pore formation (9–11). DM20 has been proposed as a differentiation factor (12, 13). A profound functional assessment of these PLP isoproteins should come from transgenic models in which either PLP or DM20 or both are absent. In this study we used homologous recombination in embryonic stem (ES) cells to replace the endogenous *Plp* gene with specific PLP and DM20 constructs. The neomycin-resistance (*neo*) gene was introduced as a selection marker in reverse orientation into intron III and was expected to be eliminated upon splicing. Here we demonstrate that the gene replacement with these constructs produced an aberrantly spliced RNA that led to a complete PLP/DM20 deficiency in myelin of CNS. Ultrastructurally the compaction of the myelin membrane system of the PLP/DM20-deficient mouse mutant is completely disrupted, leading to a reduced electric nerve conductance and impairments in neuromotor coordination and spontaneous activity.

## MATERIALS AND METHODS

**Targeting Constructs.** The vectors pPLPdel25$^{h}$neoTK and pPLPwt25$^{h}$neoTK, which contain 6.7 kb of the murine genomic *Plp* sequence, have been constructed by standard cloning techniques (14). In pPLPdel25$^{h}$neoTK, a deletion of 105 bases at the 3′ end of exon III was introduced to mimic DM20. As a selection marker, the *neo* gene of pMCIneopA (Stratagene) was cloned in reverse orientation into intron III. The thymidine kinase (*tk*) gene of pIC19r-MCI-tk was added to the 5′ end of the vectors (see Fig. 1).

**Cells.** ES cells (of cell line E14) were grown to 90% confluency on feeder layers of mitomycin C-treated G418-resistant mouse embryonic fibroblasts (15). Electroporations were performed using $10^7$ cells in 0.8 ml of phosphate-buffered saline and 20 μg of linearized replacement vector DNA in a 0.4-cm cuvette of a Bio-Rad gene pulser set at 220 V and 500 μF. G418 (250 μg; Sigma) and ganciclovir (2 μM) were added for double selection after 24 h. After 8–10 days, resistant clones were picked, expanded, and analyzed. DNA was prepared from cells lysed in 50 mM Tris·HCl, pH 7.5/100 mM NaCl/50 mM EDTA/1% SDS/proteinase K (400 μg/ml) overnight at 37°C and digested with *Hin*dIII and *Bgl* II for Southern blot analysis using the external $^{32}$P-labeled *Plp* probes plp56 and plp67 or an exon III probe, respectively (see Fig. 1). Positive clones were also checked for the homologous recombination event by PCR using the primers neoATG (*neo*-specific) and HRA (downstream *Plp* primer). The deletion of exon III was confirmed by using primers ExIIS and SauA, which flank exon III. Blastocysts of superovulated C57BL/6J and CD1 females were injected with 10–20 cells of targeted clones, and groups of 5–14 blastocysts were transferred into pseudopregnant females as described (16). Two of the injected clones yielded one germ-line chimera each. Offspring were intercrossed and genotyped to obtain homozygous transgenic lines.

**RNA Analysis.** Total RNA of 15- to 20-day-old mouse brain was extracted as described (17). Fifteen micrograms of RNA

The publication costs of this article were defrayed in part by page charge payment. This article must therefore be hereby marked "*advertisement*" in accordance with 18 U.S.C. §1734 solely to indicate this fact.

Abbreviations: PLP, proteolipid protein; CNS, central nervous system; ES, embryonic stem.

†To whom reprint requests should be addressed.

was separated on 1.5% agarose/formaldehyde gels and blotted onto BA85 nitrocellulose membranes (Schleicher & Schüll). Membranes were hybridized in 50 mM phosphate buffer, pH 6.8/5× standard saline citrate (SSC)/1× Denhardt's solution/50% (vol/vol) formamide/10% dextran sulfate/salmon sperm DNA (100 μg/ml) containing $2 \times 10^5$ cpm of $^{32}$P-labeled probe per ml at 42°C. They were washed in 0.1× SSC/0.1% SDS at 50°C.

**Myelin Analysis.** Total brain myelin protein extracts (50 μg per lane for Coomassie blue staining of gels; 5 μg per lane for silver staining) were separated on SDS/15% PAGE. For electron microscopy, anesthetized mice were perfused with 6% (vol/vol) glutaraldehyde via the left cardiac ventricle. The optic nerve was postfixed in 1% phosphate-buffered $OsO_4$ in 0.1 M sucrose and embedded in Epon 812. Ultrathin cross sections were contrasted with uranyl acetate and lead citrate and examined as described (18).

## RESULTS

**Production of PLP/DM20-Deficient Mice.** The *Plp* targeting constructs pPLPdel25$^h$neoTK and pPLPwt25$^h$neoTK contain 6.7 kb of homologous sequence: one in which a deletion of 105 bp in exon III mimicking DM20 was introduced, the other with the wild-type form of exon III (Fig. 1*A*). They both contain a *neo* gene inserted in reverse orientation into the third intron of the *Plp* gene and a *tk* gene at the 5′ end. The linearized vectors were introduced into E14 ES cells by electroporation, and one potential recombinant was identified for every 36 clones selected with G418 and ganciclovir using a Southern blot screening strategy with an external hybridization probe 3′ to the targeting construct (Fig. 1*A*). As expected for a homologous integration event, endogenous *Hin*dIII fragments were larger by 1.1 kb due to the *neo* insertion (Fig. 1*B*). In addition, the DM20 deletion of 105 bp in pPLPdel25$^h$neoTK-derived clones was detected by using an exon III-specific probe hybridizing with a 600-bp DM20-specific *Bgl* II restriction fragment, whereas the respective wild-type *Bgl* II fragment has a length of 700 bp (Fig. 1*B*). Targeted integration into the *Plp* gene was confirmed by PCR analysis using the primers neoATG and HRA, which hybridize with construct-specific *neo* sequences and sequences flanking the 3′ end of the targeting insert, respectively, giving rise to a 1.4-kb amplification product (Fig. 1*B*). The relevant exon III allele was determined by using primers ExIIS and SauA, which border the DM20 deletion and amplify a 1200-bp fragment for the wild-type and 1100 bp for the DM20 allele (Fig. 1*B*). Targeted ES cells were injected into C57BL/6J and CD1 blastocysts, and two germ-line chimeras transmitted the mutation to their offspring. One chimera contained the DM20 construct in a C57BL/6J background (dm20/neo), and the other contained the wild-type/*neo* construct in a CD1 background (plp/dm20/neo).

**RNA and Protein Analysis.** To study the effect of the *neo* cassette present in reverse orientation within intron III of the *Plp* gene on DNA transcription and RNA processing in our transgenic mice, we extracted RNA from the brains of 15- to 20-day-old homozygous and heterozygous mutant mice and wild-type control mice. Northern blots were hybridized with *Plp*-specific cDNA. Homozygous mutants of both transgenic lines showed a complete lack of the normally occurring transcripts of 1.6, 2.4, and 3.2 kb (Fig. 2*A*). However, larger transcripts hybridizing with a *neo* probe (Fig. 2*B*) and a genomic *Plp* probe (not shown) between ≈4 and 5 kb were detected in both homozygous and heterozygous mutants upon prolonged exposure. The number of these aberrant transcripts was reduced by a factor of ≈100 when the intensity of the signals was correlated with the tubulin control hybridization. The transcription pattern of the two lines of transgenic mice, dm20/neo and plp/dm20/neo, was identical. This suggests that abnormal splicing is indeed due to the insertion of the *neo* box and not due to the exon III mutation

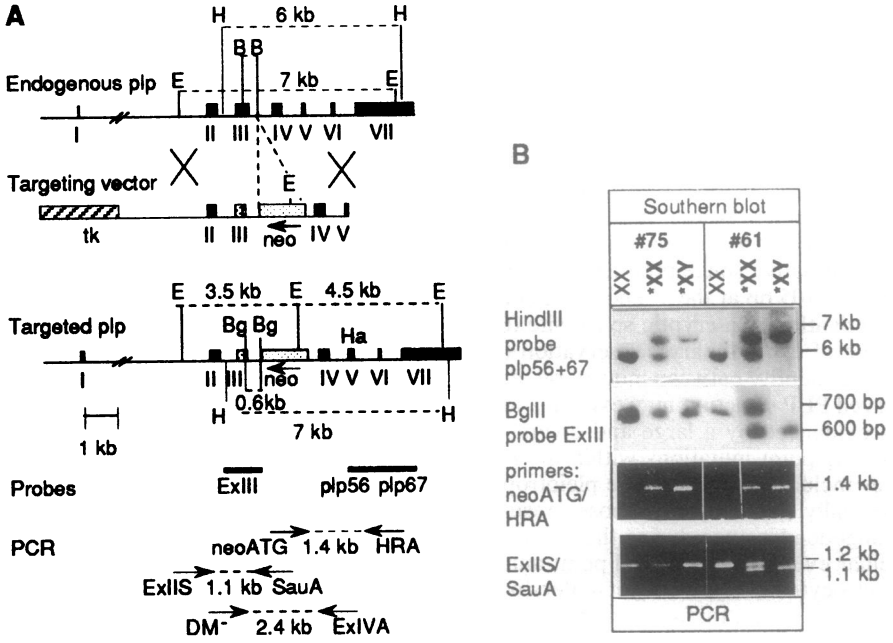


FIG. 1. *Plp* gene, targeting construct, and expected and observed homologous recombination events. (*A*) Restriction map and structure of the endogenous *Plp* gene, the targeting construct pPLPX25$^h$neoTK (X = wt25$^h$ or del25$^h$) and the targeted *Plp* locus. Numbered boxes indicate exons. E, H, Ha, and B represent cleavage sites from *Eco*RI, *Hin*dIII, *Hpa* I, and *Bgl* II, respectively. The diagnostic restriction polymorphisms and PCR products are indicated together with the location of external and internal probes (thick bars) for Southern blot analysis and the location of analytical PCR primers (arrows) with their respective amplification products. (*B*) Genotype analysis of the transgenic lines 61 (dm20/neo) and 75 (plp/dm20/neo). (*Upper*) Southern blot analysis: *Hin*dIII digestion followed by hybridization with the external probes plp56 and plp67 and *Bgl* II digestion followed by hybridization with the internal exon III probe. (*Lower*) PCR analysis: neoATG/HRA probing for the homologously integrated *neo* cassette in intron III and ExIIS/SauA probing for the presence of the DM20 deletion. Genotypes are indicated as XX for wild-type female, *XX for heterozygous mutant female, and *XY for hemizygous mutant male mice.

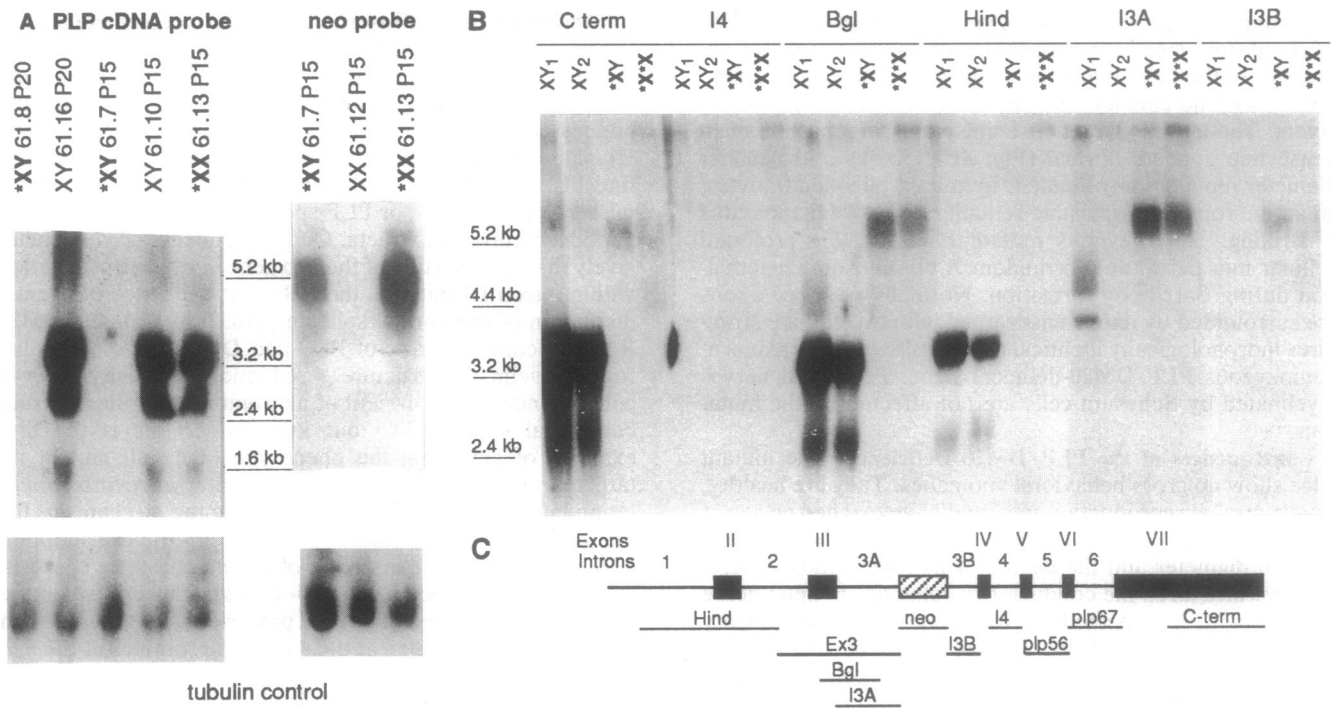


FIG. 2. Northern blot analysis of total mouse brain RNA. (*A*) Total RNAs from dm20/neo mice (61.7, 61.8, 61.13) hetero- and homozygous for the respective allele and the wild-type control probes (61.10, 61.12, 61.16) were size-fractionated on a 1.5% agarose/formaldehyde gel, blotted to a nitrocellulose membrane, and hybridized to a $^{32}$P-labeled rat *Plp* cDNA probe (−74 to 298 bp) and an 800-bp *Pst* I *neo* probe. Films were exposed for 24 h (*Left*) and 72 h (*Right*). Blots were reprobed with α-tubulin (*Lower*). Genotypes are as in Fig. 1. The ages of the mice are indicated with P15 and P20 for 15 and 20 postnatal days. (*B*) Transcripts of the *Plp* gene were mapped using hybridization probes C-term, I4, Bgl, Hind, I3A, and I3B as indicated in *C*. Twenty micrograms of total RNA from adult C57BL/6 males ($XY_1$), CD1 males ($XY_2$), transgenic dm20/neo males (*XY), and plp/dm20/neo females (*X*X) were separated on a 1.5% formaldehyde/agarose gel and blotted to a nitrocellulose membrane. (*C*) Location of probes used for Northern blot analysis.

introduced by the targeting vector into the dm20/neo mice. The structure of these aberrant transcripts was more precisely analyzed by mapping with probes for different introns and exons as summarized in Fig. 2 *B* and *C*. These transcripts hybridized to the *neo* probe and to probes containing intron IIIA (Bgl, I3A, Ex3) or intron IIIB (I3B) and furthermore to the 3′-terminal 1535-bp untranslated sequence of exon VII (C-term probe) of *Plp* cDNA. The hybridization pattern with the intron- and exon-specific probes, outlined in Fig. 2*C*, proves that intron III of the primary transcripts of the mutant mice with its inserted *neo* box is skipped during splicing. The structure of these aberrant mRNA is, therefore, exons I–II–III–intron IIIA–*neo*–intron IIIB–exons IV–V–VI–VII with estimated sizes of 5.2 and 4.4 kb (900 bp of intron III plus the 1100-bp *neo* gene added to the normally spliced 3.2- and 2.4-kb transcripts). The lack of the normal PLP transcripts leads to a complete deficiency of PLP and DM20 proteins. No PLP and DM20 bands were detectable in the protein pattern of the myelin samples of homozygous transgenic mice in silver-stained SDS/PAGE gels (Fig. 3). By Western blot analysis using PLP-specific antibodies, no PLP or DM20 signals were detected (data not shown). The open reading frame of the aberrant high molecular mass RNA would yield products consisting of the coding sequences of exons I, II, and III and nine additional triplets of intron III, terminated by two stop codons. However, these hypothetical truncated PLPs with expected molecular masses of 17 and 13 kDa were not detected in silver-stained gels or upon immunoblotting. Thus, in terms of RNA and protein expression, our two homozygous lines of transgenic mice are both PLP- and DM20-deficient.

**Disrupted Myelin Ultrastructure.** The morphological consequences for the molecular architecture of the myelin sheath devoid of its integral membrane proteins PLP and DM20 became apparent in electron microscopy of the corpus callosum, spinal cord, and optic nerve as representative samples of the CNS. The compact myelin membrane multilayer around wild-type axons contrasts with that of the homozygous mutant mice, with optic nerve cross sections shown as

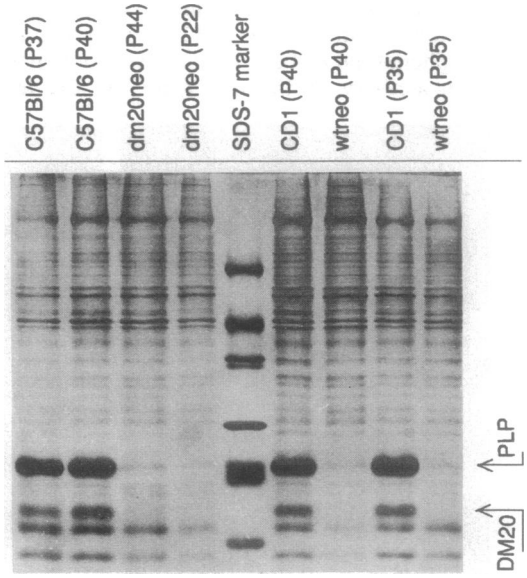


FIG. 3. Silver-stained SDS/PAGE (15%) protein analysis of CNS myelin proteins of wild-type C57BL/6 and CD1 and homozygous mutant dm20/neo (dm20neo) and plp/dm20/neo (wtneo) mice. Isolated myelin is completely devoid of PLP and DM20 in homozygous PLP/DM20-deficient mutants. The age of the sacrificed animals is indicated in postnatal days.

an example (Fig. 4). In homozygous PLP/DM20-deficient mice, plasma membrane processes of oligodendrocytes address only the large diameter axons and wrap them voluminously with no contact between the external surfaces of the layers. The intermediate dense line is missing, but the main dense line appears normal (Fig. 4*C*). Axons with smaller diameter remain unmyelinated. In mutant oligodendrocytes, an active rough endoplasmic reticulum and Golgi apparatus is striking. Heterozygous mutant mice show a profound cellular mosaicism due to random X chromosome inactivation during Barr body formation. Normally wrapped axons are surrounded by axons ensheathed with myelin-like structures morphologically identical to structures around axons of homozygous PLP/DM20-deficient mice. Peripheral nerves myelinated by Schwann cells are not affected by the mutation.

**Consequences of the PLP/DM20 Deficiency.** The mutant mice show no gross behavioral anomalies. They are healthy, have a normal reproduction rate, and have reached an age of 9 months so far. Electrical nerve conductance is proportional to axon diameter and the degree of its myelination. Therefore, we measured the conductance velocities in optic nerve preparations. As expected, we found a conductance velocity reduced to about half the normal value in PLP/DM20-deficient mice (data not shown). Specialized behavioral tests revealed an impairment of neuromotor coordination in PLP/DM20-deficient mice. In Rota Rod tests, wild-type mice were able to hold on to the rotating rod significantly longer and at higher revolution rates than the mutant mice. Open field tests (19), which quantify the spontaneous locomotor activity, clearly indicate a reduced activity of homozygous PLP/DM20-deficient mice and a strongly reduced spontaneity in their horizontal activity. We interpret these behavioral deficits as a direct consequence of the reduction of the compound action potential velocities found in transgenic mice.

## DISCUSSION

By targeting the *Plp* gene, we produced two independent lines of transgenic mice, dm20/neo and plp/dm20/neo (as a control), both carrying a *neo* gene cassette within intron III of the *Plp* gene. The dm20/neo mutant carries a 105-bp deletion in exon III, mimicking DM20, which was not expressed; the phenotype of both mutants was dominated by the disrupting activity of the *neo* gene. At the level of transcription, the *neo* insertion causes (*i*) a complete lack of the normally spliced and translatable transcripts of 1.6, 2.4, and 3.2 kb and (*ii*) a strongly reduced transcription of the mutated *Plp* gene to 4.4- and 5.2-kb mRNAs containing the coding sequence of the seven exons of the *Plp* gene and intron III including the *neo* cassette. On the protein level, we did not find PLP, DM20, a hypothetical translation product with a missense C terminus, or PLP-specific immunoreactive polypeptides in myelin extracts. Our experiments prove conclusively that the insertion of the *neo* gene in reverse orientation within intron III initiated the following sequence of events: disruption of the normal splicing pattern of PLP and DM20 RNA → complete lack of PLP and DM20 proteins → disrupted myelin ultrastructure → reduction of velocity of nerve conductance → impairment of neuromotor coordination and behavioral changes. To our knowledge, this is the first example of achieving the phenotype of a null mutant by targeted integration of a selection marker in reverse orientation into an intron of a gene. What are the mechanisms for the qualitative and quantitative changes in the transcription of the *Plp* gene? The insertion of the *neo* cassette causes a splicing defect, which leads to 4- to 5-kb transcripts. On the basis of our analytical data, we propose the synthesis of an antisense RNA initiated at the strong *tk* promoter of the *neo* gene leading to the formation of double-stranded RNA. Double-stranded RNAs are believed to be rapidly degraded by nucleases (20–22) with the complete lack of the translation product. Further experiments will prove whether the observation reported here would be a general strategy for silencing gene expression. The two transgenic PLP/DM20-deficient lines show an identical phenotype. Electron microscopy reveals severe structural alterations in the myelin sheaths of axons of CNS. The plasma membrane processes of oligodendrocytes of mutant mice target only axons with a large diameter and wrap them with an irregular voluminous multimembrane system. Compaction in the major dense line is not affected, but the intraperiod dense line is missing completely. Small axons remain un- or hypomyelinated. The lipid composition of the myelin bilayer with its polar head groups is unaltered (analysis not shown). Therefore homophilic or heterophilic interactions of apposed surfaces of extracytosolic loops of PLP must be responsible for compaction of extracytoplasmic surfaces of oligodendrocyte plasma membrane processes. Oligodendrocytes of heterozygous mutant mice show a profound cellular mosaicism, which is docu-

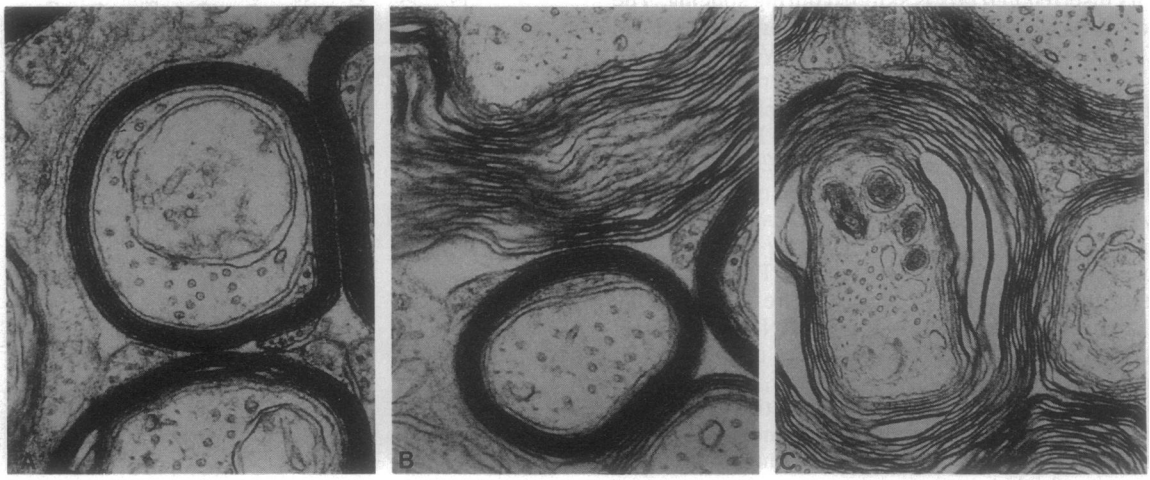


FIG. 4. Electron micrographs of cross sections of the optic nerve of dm20/neo mice (age 29 days). (*A*) Wild-type (XY). Only myelinated axons are visible in this micrograph. The myelin sheaths show a regular compaction visible as major and intraperiod dense lines. (*B*) Heterozygous mutant (*XX). Mosaicism of normally myelinating and loosely wrapping oligodendrocytes due to random X chromosome inactivation is shown. (*C*) Hemizygous mutant (*XY). Noncompacted voluminously distorted myelin sheaths around large diameter axons. Small diameter axons remain unmyelinated. (×43,200.)

mented by the electron micrographs of heterozygous females: regularly myelinated axons are embedded in areas containing only loosely myelinated axons. Myelination of peripheral nerves was not affected by our PLP mutations. Electric nerve conductance is proportional to the diameter of axons and their degree of myelination. In agreement with the morphology of their myelin sheaths, optic nerves of PLP/DM20-deficient mice show a reduction of their action potential velocities by 50%. Despite the drastically altered myelin ultrastructure, our transgenic mice show no gross behavioral anomalies. They are fertile with a normal reproduction rate. However, severe defects of neuromotor coordination and a loss of spontaneous activity in their behavior become apparent in specialized tests. The relatively mild symptoms compared with the intense ultrastructural and electrophysiological perturbations of our PLP/DM20-deficient mice raises the exciting question of how the complete loss of structure and function of PLP in our PLP/DM20-deficient mouse mutant can be reconciled with the survival of oligodendrocytes, with the high degree of evolutionary conservation, and with life in general, whereas most point mutations within exons of the *Plp* gene lead to apoptosis of oligodendrocytes and the death of the affected individual. We conclude from our PLP/DM20-deficient mouse model that the absence of the integral isoproteins PLP and DM20 in the myelin membrane clearly precludes the premature death of oligodendrocytes. Our working hypothesis is that *Plp* point mutations lead to respective missense proteins with altered conformations, which are either incompatible with the assembly of the myelin membrane or perturb cellular membrane trafficking. The extremely hydrophobic membrane domains of the PLP isoproteins are scarcely degradable by proteases as experienced in biochemical studies (1, 2). Their accumulation and aggregation as "hydrophobic junk" may cause cell death. Our experiments convincingly define the function of PLP/DM20 for the structural integrity of myelin: the PLP isoproteins are responsible for myelin compaction and the large increase in electrical conductance properties of the tightly wrapped axons in CNS. They provide a great selection advantage in evolutionary processes. They are the prerequisites for the compact structure of CNS as a whole. During myelinogenesis, oligodendrocyte maturation in the PLP/DM20-deficient mouse does not require the expression of the *Plp* gene. If the proposed regulatory functions of PLP or DM20 during embryonic development are correct, they may be compensated by redundant functions of other proteins. Life and reproduction are compatible with a structurally altered myelin sheath devoid of its major polytopic membrane proteins PLP and DM20. Our PLP/DM20-deficient mouse model will be an important tool for future investigations concerning the axon–oligodendrocyte interaction during myelinogenesis and the molecular events in myelin diseases.

We are grateful to Professor Büssow, Anatomisches Institut, Universität Bonn, for excellent collaboration in performing electron microscopy and Dr. Rafael Gutierrez for measuring the conductance velocity of optic nerves. We thank R. Müller and B. Gassen for skilled technical assistance. This work was generously supported by the Fritz Thyssen Stiftung, Hertie-Stiftung, and the Deutsche Forschungsgemeinschaft, SFB 243.

1. Stoffel, W., Hillen, H. & Giersiefen, H. (1984) *Proc. Natl. Acad. Sci. USA* **81**, 5012–5016.
2. Weimbs, T. & Stoffel, W. (1992) *Biochemistry* **31**, 12289–12296.
3. Derry, J. M. & Barnard, P. J. (1991) *Genomics* **10**, 593–597.
4. Diehl, H.-J., Schaich, M., Budzinski, R.-M. & Stoffel, W. (1986) *Proc. Natl. Acad. Sci. USA* **83**, 9807–9811.
5. Schaich, M., Budzinski, R.-M. & Stoffel, W. (1986) *Biol. Chem. Hoppe Seyler* **367**, 825–834.
6. Nave, K.-A., Lai, C., Bloom, F. E. & Milner, R. J. (1987) *Proc. Natl. Acad. Sci. USA* **84**, 5665–5669.
7. Schliess, F. & Stoffel, W. (1991) *Biol. Chem. Hoppe Seyler* **372**, 865–874.
8. Pham-Dinh, D., Boespflug-Tanguy, O., Mimault, C., Cavagna, A., Giraud, G., Leberre, G., Lemarec, B. & Dautigny, A. (1993) *Hum. Mol. Genet.* **2**, 465–467.
9. Inouye, H. & Kirschner, D. A. (1991) *J. Neurosci. Res.* **28**, 1–17.
10. Doyle, J. P. & Colman, D. R. (1993) *Curr. Opin. Cell Biol.* **5**, 779–785.
11. Kitagawa, K., Sinoway, M. P., Yang, C., Gould, R. M. & Colman, D. R. (1993) *Neuron* **11**, 433–448.
12. Ikenaka, K., Kagawa, T. & Mikoshiba, K. (1992) *J. Neurochem.* **58**, 2248–2258.
13. Timsit, S. G., Bally-Cuif, L., Colman, D. R. & Timsit, B. (1992) *J. Neurochem.* **58**, 1172–1175.
14. Sambrook, J., Fritsch, E. F. & Maniatis, T. (1989) *Molecular Cloning: A Laboratory Manual* (Cold Spring Harbor Lab. Press, Plainview, NY).
15. Robertson, E. J. (1987) in *Teratocarcinomas and Embryonic Stem Cells: A Practical Approach*, ed. Robertson, E. J. (IRL, Oxford), pp. 71–112.
16. Bradley, A., Evans, M., Kaufman, M. & Robertson, E. (1984) *Nature (London)* **309**, 255–256.
17. Chomczynski, P. & Sacchi, N. (1987) *Anal. Biochem.* **162**, 156–159.
18. Büssow, H. (1978) *J. Neurocytol.* **7**, 207–214.
19. Broadhust, P. L. (1957) *Br. J. Stat. Psychol.* **48**, 2–12.
20. Murray, J. A. H. (1992) *Antisense RNA and DNA* (Wiley–Liss, New York).
21. Nellen, W. & Lichtenstein, C. (1993) *Trends Biochem. Sci.* **18**, 419–423.
22. Pontius, B. W. & Berg, P. (1990) *Proc. Natl. Acad. Sci. USA* **87**, 8403–8407.